2016 13th International Conference on Electrical Engineering, Computing Science and Automatic Control (CCE), Mexico, City. Mexico. September 26-30, 2016.

Simulation of a Double-stage Micro-Inverter for Grid-Connected Photovoltaic Modules

Jose Luis Diaz-Bernabe
Electrical Engineering Department
CINVESTAV I.P.N.
México City, México
jldiaz@cinvestav.mx

Arturo Morales-Acevedo
Electrical Engineering Department
CINVESTAV I.P.N.
México City, México
amorales@solar.cinvestav.mx

***Abstract*— In this work, the performance of a double-stage micro-inverter using the adaptive incremental conductance (*AIC*) algorithm for grid-connected photovoltaic (PV) modules is evaluated by means of a Simulink model. We observe the response of the micro-inverter under transients of solar irradiance and under static conditions. We show that Maximum Power Point Tracking (MPPT) and conversion efficiencies above 98% can be expected.**

Keywords— Adaptive maximum power point tracking; grid-connected PV systems simulation; DC-AC power conversion

I. NOMENCLATURE

v	PV module instantaneous voltage
i	PV module instantaneous current
p	PV module instantaneous power
p_{max}	PV module ideal power
d_k	Duty cycle of DC-DC converter
D_{step}	Constant correction term for duty cycle
G_V	Generalized conductance function
MPPT	Maximum power point tracking
AIC	Adaptive Incremental conductance
v_{dc}	DC-Link voltage
i_g	Grid current
v_g	Nominal grid voltage
L_g	Equivalent grid inductance
R_g	Equivalent grid resistance
SPWM	Sinusoidal pulse width modulation
PI	Proportional e integral

II. INTRODUCTION

A micro-inverter is a low power photovoltaic (PV) inverter attached to a single PV module. The PV module produces alternating current (AC) instead of direct current (DC). Because of its relatively low cost and modular design, several micro-inverters can be connected in a parallel form to increase the power rating. Unlike the string inverter where a single Maximum Power Point Tracking (MPPT) control is dedicated to a number of PV modules, a micro-inverter implements a Maximum Power Point Tracking (MPPT) control for every PV module, and therefore partial shading conditions are not a severe matter.

A double-stage grid connected micro-inverter is shown in Fig. 1 [1]. In this layout the DC-DC stage shall provide the amplification of the PV voltage and the MPPT control for the PV source. The MPPT block increases the overall PV system efficiency by making the PV module to work at the optimized operating point. In the single-loop MPPT structure control, at time step k, the current i and voltage v signals enter the MPPT controller and then outputs a value for the duty cycle d_k. The DC-AC stage provides interconnection with the utility and its basic tasks are: to produce an alternating current i_g with a total harmonics distortion (THD) lower than 5% [2], to inject the current to the grid, to synchronize with the grid at a nominal frequency, and to isolate by itself during the grid transients.

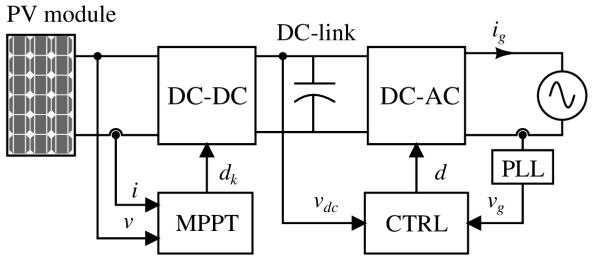

Fig. 1. Double stage micro-inverter.

Maximum power point tracking (MPPT) methods maximize the output power in photovoltaic (PV) systems. The MPPT method is a part of control configuration of a DC-DC converter attached at the terminals of PV array. A number of MPPT algorithms suggested for autonomous and grid connected PV systems have been reviewed in [3], [4], [5], [6], [7], [8]. Based on the power versus voltage curve of a PV array, the Perturb and Observe (P&O) algorithm takes the PV array operating point near the maximum power point by verifying the slope of the power as a function of the voltage (dp/dv). A duty cycle correction term (D_{step}) is added or subtracted from the current one d_k depending upon the sign of dp/dv. The Incremental Conductance (IC) method compares the incremental conductance (di/dv) with the negative of the instantaneous conductance (i/v) to decide if D_{step} is added or subtracted from the current duty cycle d_k [9]. At the maximum power point $di/dv = -i/v$. Lately, it was proved by D. Sera et al. [10] that both P&O and IC conventional algorithms have an equivalent behavior under similar dynamic conditions.

The conventional algorithms depicted above, produces power oscillations around the maximum power point (MPP) because they use a constant correction factor D_{step}. N. Femia et al. [11] proposed a method to optimize the sampling period and the constant correction term for conventional algorithms. The

978-1-5090-3511-3/16/$31.00 ©2016 IEEE

Adaptive MPPT algorithms have been expanded to enhance the MPP tracking speed under dynamic conditions and to reduce the power oscillations around the MPP under steady state conditions [12], [13], [14], [15], [16], [17], [18], [19], [20], [21], [22]. In a preceding paper [21], the correct definition for the adaptive incremental conductance (AIC) algorithm for a single-loop MPPT control structure was proposed. In this algorithm, the adaptive correction term is determined by the total generalized conductance ($G_V = di/dv + i/v$).

In this paper the performance of a double-stage grid-connected PV micro-inverter with the adaptive incremental conductance algorithm is evaluated. The AIC algorithm developed in [21] is used in a single-loop MPPT control structure. With this purpose, in section III, the correct AIC algorithm will be described concisely. Then, in section IV the DC-DC and DC-AC stages are described. In section V, the analysis of the control system for the grid current and DC-link voltage is illustrated. In section VI, the performance of the grid-connected micro-inverter with the AIC algorithm is presented by means of simulation results. The performance is estimated by evaluating the MPPT efficiency, the power conversion efficiency and the total harmonic distortion for the grid current. It will be shown that the AIC algorithm achieves good steady state and dynamic MPPT efficiencies, around 99% and the overall conversion efficiency is larger than 98%.

III. ADAPTIVE INCREMENTAL CONDUCTANCE

The power of a PV array under a nominal solar irradiation is $p = i.v$, and its derivative with respect to the voltage at the maximum power point is:

$$\left.\frac{dp}{dv}\right|_{MPP} = i + v\frac{di}{dv} = v.G_V = 0 \tag{1}$$

where the function G_V is:

$$G_V = \frac{i}{v} + \frac{di}{dv} \tag{2}$$

the first term at the right is the instantaneous conductance and the second term is the incremental conductance. In a former paper [21] G_V was chosen as an adaptive rule to adjust the correction term for the AIC algorithm and it has units of Ω^{-1}. Therefore, the AIC algorithm modifies the duty cycle at time step k according to:

$$d_k = d_{k-1} - N_{AIC}.G_V \tag{3}$$

where N_{AIC}, expressed in units of Ω, is a factor that must be optimized. This method requires both the incremental conductance and the instantaneous conductance to be evaluated.

IV. MODELING THE DC-DC AND DC-AC STAGES

Several power electronics structures for the DC-DC and DC-AC stages had been proposed for their use in the double-stage PV micro-inverters [1], [23]. In this work an isolated, high efficiency flyback converter accomplishes the DC-DC stage and a full-bridge voltage source inverter performs the DC-AC stage.

A. DC-DC stage

The DC-DC stage of the double-stage PV micro-inverter is analyzed with the scheme shown in Fig. 2. This diagram contains a PV module, a flyback converter and MPPT control block. The flyback converter features a reduced components number and high power conversion efficiency at related power levels. The high frequency transformer offers galvanic isolation between PV source and the grid interface. At the output of the flyback, the capacitor C holds the high level DC-link voltage for the DC-AC stage. The effect of the nominal grid current on the DC-DC converter is represented by an equivalent resistance R.

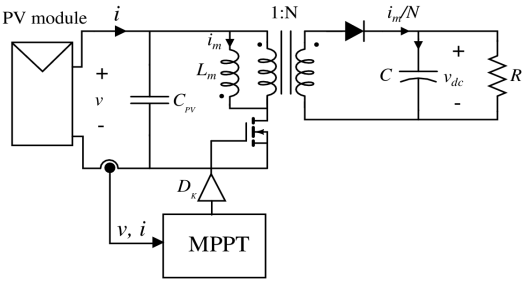

Fig. 2. The DC-DC stage.

The circuit shown in Fig. 3 models the PV module [24]. The effects of the solar irradiance and cell temperature on the output current are included. The output current i as a function of v is approximated by:

$$i = i_L - i_0\left(\exp\left(\frac{v + iR_S}{AN_S v_{TH}}\right) - 1\right) - \frac{v + iR_S}{R_P} \tag{4}$$

where A, R_S, R_P, I_0 and I_L are parameters depending of the particular PV module.

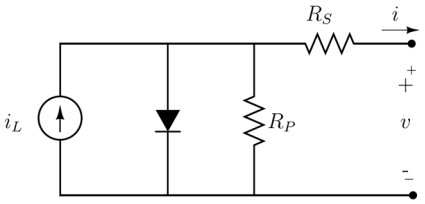

Fig. 3. PV module equivalent circuit [24].

Some important techniques for modeling and simulating switched mode DC-DC converters are revised by D. Maksimovic et al [25]. The behavior of the flyback converter in continuous current mode (CCM) is estimated by its state space average model [26]:

978-1-5090-3511-3/16/$31.00 ©2016 IEEE

$$\begin{aligned}\frac{d}{dt}v &= \frac{1}{C_{PV}}\left(i - i_m D\right)\\ \frac{d}{dt}i_m &= \frac{1}{L_m}\left(v.D - \frac{1-D}{N}v_{dc}\right)\\ \frac{d}{dt}v_{dc} &= \frac{1}{C}\left(\frac{1-D}{N}i_m - \frac{1}{R}v_{dc}\right)\end{aligned} \tag{5}$$

where v, i_m and v_{dc} are the state variables, i is the input variable, D is the control variable, and the terms C_{PV}, L_m, N and C are parameters of the converter. We have assumed that the flyback is fed by the current i coming from PV module.

B. DC-AC stage

The grid connected DC-AC stage is shown in Fig. 4. The inductor L and capacitor C establish a low pass filter, L_g and R_g model the equivalent grid impedance and v_g is the utility nominal voltage. In order to allow power flowing from PV module toward the utility, the instantaneous voltage $v_{dc}(t)$ must be greater than instantaneous $v_g(t)$. The voltage v_{dc} coming from the DC-DC stage must be regulated to a constant value with relatively small ripple, but on special cases a large voltage ripple is permissible to reduce the DC-link capacitor. A control technique, as those described in [27], [28], [29], and [30] rejects the large voltage ripple and distortion on the current i_g.

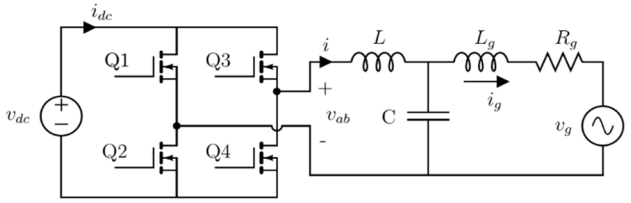

Fig. 4. The DC-AC stage.

The DC-AC stage is analyzed by means of the reduced circuit of Fig. 5. In unipolar SPWM the voltage v_{ab} is proportional to the modulating signal v_{ctrl} [31], [32]:

$$v_{ab} = \frac{V_{dc}}{\hat{V}_c}v_{ctrl} \tag{6}$$

where $\hat{V}_c$ is the peak value of a triangular signal carrier. The behavior in the time domain of the circuit of Fig. 5 can be approximated by equations (7):

$$\begin{aligned}L\frac{d}{dt}i &= v_{ab} - v_C - iR_L\\ C\frac{d}{dt}v_C &= i - i_g\\ L_g\frac{d}{dt}i_g &= v_c - v_g - i_g R_g\end{aligned} \tag{7}$$

where v_C is the voltage on the capacitor C, and R_L models the average resistance across Q1-Q4 and the serial resistance of L.

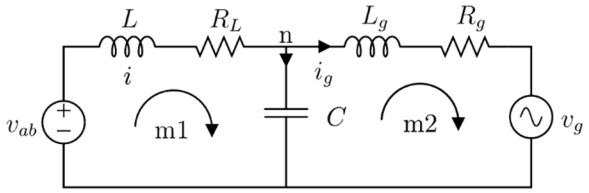

Fig. 5. Equivalent circuit for the DC-AC stage.

V. Control System

Double-stage grid-connected PV micro-inverters requires to regulate the voltage at the DC-link and the grid current. In this work a couple of PI controllers are employed for voltage and current loops.

A. Current control loop

Fig. 6 displays a classical PI control with grid voltage feed-forward for current control. The G_{CI} is represented by a proportional-integral controller [33]:

$$G_{CI} = K_P + \frac{K_I}{s} \tag{8}$$

The transfer function for the plant is [29]:

$$G_P(s) = \frac{V_{dc}}{\hat{V}_c}\cdot\frac{1}{sL + R_L} \tag{9}$$

and the feed-forward gain FF is described by:

$$FF = \frac{\hat{V}_c}{V_{dc}} \tag{10}$$

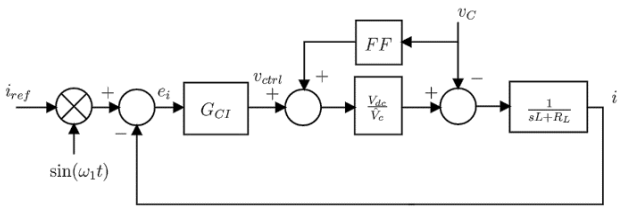

Fig. 6. Block diagram for the current control loop [29].

B. DC-Link voltage control loop

The DC-Link capacitor is chosen to compensate the maximum permissible voltage ripple ΔV_{dc}. Equation (11) is adequate to estimate the link capacitor [34]:

$$C = \frac{P}{2\omega_1 V_{dc}\Delta V_{dc}} \tag{11}$$

where P is the maximum power, ω_1 is the fundamental frequency in rad/sec and V_{dc} is the average DC-link voltage. A reasonable design is to keep the voltage ripple less than 5 % of the average DC-link voltage [28].

978-1-5090-3511-3/16/$31.00 ©2016 IEEE

A diagram of the voltage control loop is shown in Fig. 7. The current loop bandwidth is two or more orders of magnitude greater than the voltage one, so it is represented by a unity gain. The G_{CV} denotes a PI controller used to regulate the voltage. The cross-over frequency is usually selected to be less than 30 Hz in order to diminish the 120 Hz component on the DC-link. The variations of the voltage at DC-link due to variations in the grid reference current are determined by:

$$G_P(s) = \frac{V_{dc}(s)}{I(s)} = -\frac{V_g}{sCV_{dc}} \tag{12}$$

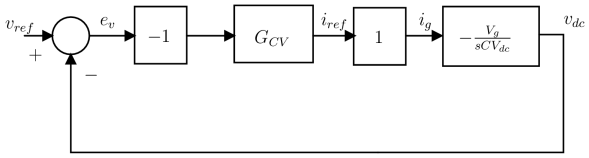

Fig. 7. Block diagram for the voltage control-loop [29].

VI. Simulation Results

The behavioral simulation of the micro-inverter with the AIC algorithm is shown in this section. The relations (4), (5) and (7) were used to build the Simulink model shown in Fig. 8 for the whole micro-inverter.

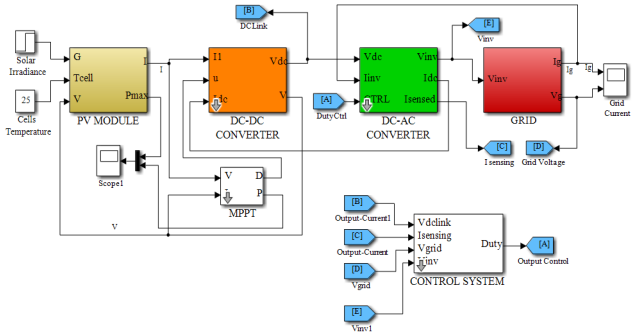

Fig. 8. Simulink model of the proposed micro-inverter

Table I shows the parameters of a 250 W PV module under STC. The five unknown terms of equation (4) were estimated with the procedure explained in [35], and they are presented in Table II. Table III displays the specifications of the flyback converter for continuous current mode operation.

TABLE I. PARAMETERS OF A 250 W PV MODULE

PARAMETER	SYMBOL	VALUE
Short circuit current	I_{SC}	8.52 A
Open circuit voltage	V_{OC}	37.30 V
Current at MPP point	I_M	8.04 A
Voltage at MPP point	V_M	30.5 V
Series cell number	N_S	60

TABLE II. ESTIMATED TERMS FOR THE PV MODULE

PARAMETER	SYMBOL	VALUE
PV module diode quality factor	A	1.04
Series resistance	R_S	0.243 Ω
Parallel resistance	R_P	1155 Ω
Photocurrent	I_L	8.52 A
Diode dark current	I_0	7.44×10^{-10} A

TABLE III. FLYBACK CONVERTER SPECIFICATIONS

PARAMETER	VALUE
N	5
L_m	100 x 10^{-6} H
C	220 x 10^{-6} F
C_{PV}	150 x10^{-6} F

The physical parameters for the DC-AC converter are shown in Table IV. We suppose a switching frequency of 3.06 KHz to produce lower switching losses. The resonant frequency for the LC filter is around 1.12 KHz.

TABLE IV. DC-AC CONVERTER SPECIFICATIONS

PARAMETER	VALUE
F_s	3.06 KHz
L	6.8 mH
C	3.0 µF
L_g	0.1 mH
R_g	1.00 Ω

At time t = 55 ms, the solar irradiance jumps from 0.7 suns up to 1.0 sun. Fig. 9 shows the dynamic response of the AIC algorithm, where a fast power tracking is observed on the transient edge and no noticeable power oscillations appear under constant irradiance conditions. The simulation sampling period T_S was 0.001 seconds and the scaling factor N_{AIC} was 0.01 Ω.

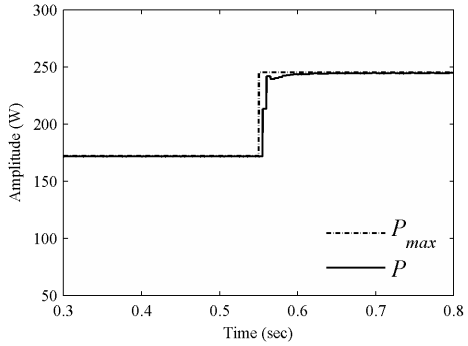

Fig. 9. Dynamic behavior of the AIC algorithm.

Fig. 10 shows the voltage at the DC-Link. Because of a large constant time, the voltage stabilizes after a relatively large settle time. Fig. 11 exhibits the grid current. Since a phase margin of 75° was used, the grid current quickly stabilizes and oscillations are not observed.

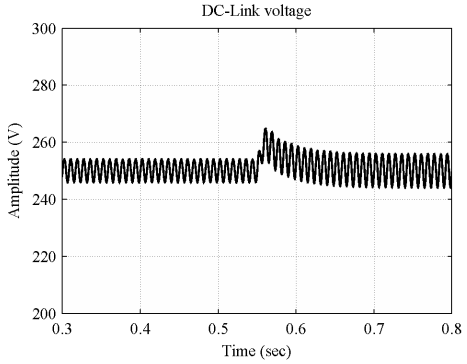

Fig. 10. Voltage regulation at the DC-link.

One important parameter for the evaluation of the performance of the MPPT algorithms is the so named MPPT efficiency defined as:

$$\eta_{MPPT} = \frac{\int_0^T p(t)\,dt}{\int_0^T p_{max}(t)\,dt} \tag{13}$$

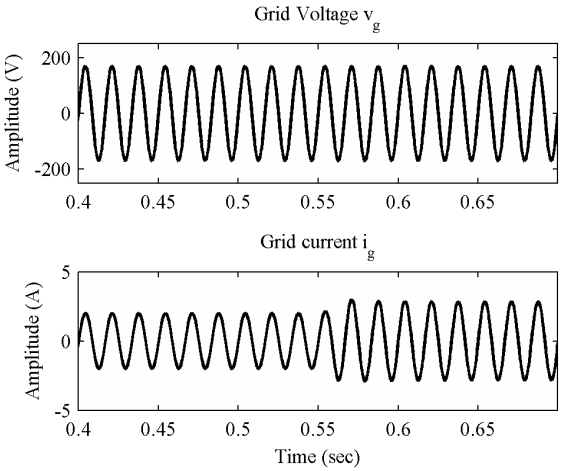

Fig. 11. Waveforms for the grid voltage and grid current.

where $p(t)$ is the power of the PV module with the MPPT control, $p_{max}(t)$ is the maximum power that the module would deliver and T is the time period of the dynamic evaluation.

Table V shows the efficiencies of the simulated PV micro-inverter. The MPPT dynamic efficiency was evaluated with the expression given in (13). The η_{conv} is an approximation for the overall power conversion efficiency. It considers only the losses due to the series resistance of the inductor and the transistors. This number would be reduced because switching loses appears in almost all switching devices and is depending on frequency.

TABLE V. MEASURED EFFICIENCIES

PARAMETER	VALUE
η_{MPPT}	98.94 %
η_{conv}	96.50 %
THD	< 1.0 %

In summary, the proposed micro-inverter, working with the AIC algorithm for MPPT, provides good expected efficiencies and then it can be implemented in a practical circuit, as we shall do in the near future.

VII. CONCLUSION

The simulation of a double-stage PV micro-inverter with the adaptive incremental conductance in a single-loop MPPT structure was shown. A fast tracking of the optimized operating point was noticed during solar irradiance transients and no power oscillations were observed on steady state conditions, and so the MPPT efficiency is high compared to conventional non-adaptive algorithms. The MPPT strategy helps to increase the overall PV system efficiency because the power of the PV module is maximized and more power is offered. The interconnection of the micro-inverter to the grid utility was modeled and simulated. A couple of PI controllers were used to regulate the voltage at the DC-link and the grid current. The overall conversion efficiency was estimated, but this number may be reduced because switching losses.

ACKNOWLEDGEMENT

José Luis Díaz-Bernabé thanks CONACYT for supporting his Ph. D. scholarship.

REFERENCES

[1] S. Kjaer, J. Pedersen and F. Blaabjerg, “A review of single-phase grid-connected inverters for photovoltaic modules”, *IEEE Transactions on Industry Applications,* vol. 41, nº 5, pp. 1292-1306, sept.-oct. 2005.

[2] "IEEE Application Guide for IEEE Std 1547(TM), IEEE Standard for Interconnecting Distributed Resources with Electric Power Systems", *IEEE Std 1547.2-2008,* pp. 1-217, April 2009.

[3] D. Hohm and M. Ropp, “Comparative Study of Maximum Power Point Tracking Algrithms”, *Progress in photovoltaics: Research and applications,* vol. 11, pp. 47-62, 2003.

[4] T. Esram and P. Chapman, “Comparison of Photovoltaic Array Maximum Power Point Tracking Techniques”, *IEEE Transactions on Energy Conversion,* vol. 22, nº 2, pp. 439-449, 2007.

[5] V. Salas, E. Olías, A. Barrado and A. Lázaro, “Review of the maximum power point tracking algorithms for stand-alone photovoltaic systems”, *Solar Energy Materials and Solar Cells ,* vol. 90, nº 11, pp. 1555-1578, 2006.

[6] M. de Brito, L. Galotto, L. Sampaio, G. de Azevedo e Melo and C. Canesin, “Evaluation of the Main MPPT Techniques for Photovoltaic Applications”, *IEEE Transactions on Industrial Electronics,* vol. 60, nº 3, pp. 1156-1167, 2013.

[7] B. Subudhi and R. Pradhan, “A Comparative Study on Maximum Power Point Tracking Techniques for Photovoltaic Power Systems”, *IEEE Transactions on Sustainable Energy,* vol. 4, nº 1, pp. 89-98, Jan. 2013.

[8] S. Jain and V. Agarwal, “Comparison of the performance of maximum power point tracking schemes applied to single-stage grid-connected photovoltaic systems”, in *IET Electric Power Applications,* vol. 1, nº 5, pp. 753-762, 2007.

[9] K. Hussein, I. Muta, T. Hoshino and M. Osakada, “Maximum photovoltaic power tracking: an algorithm for rapidly changing atmospheric conditions”, *IEE Proceedings-Generation, Transmission and Distribution,* vol. 142, nº 1, pp. 59-64, 1995.

[10] D. Sera, L. Mathe, T. Kerekes, S. V. Spataru and R. Teodorescu, "On the Perturb-and-Observe and Incremental Conductance MPPT Methods for PV Systems", *IEEE Journal of Photovoltaics,* vol. 3, nº 3, pp. 1070-1078, July 2013.

[11] N. Femia, G. Petrone, G. Spagnuolo and M. Vitelli, "Optimization of perturb and observe maximum power point tracking method", *IEEE Transactions on Power Electronics,* vol. 20, nº 4, pp. 963-973, 2005.

[12] Weidong Xiao and W. G. Dunford, "A modified adaptive hill climbing MPPT method for photovoltaic power systems", *2004 IEEE 35th Annual Power Electronics Specialists Conference,* 2004, vol.3, pp. 1957-1963.

[13] P. J. Wolfs and L. Tang, "A Single Cell Maximum Power Point Tracking Converter without a Current Sensor for High Performance Vehicle Solar Arrays", *2005 IEEE 36th Power Electronics Specialists Conference, Recife, 2005,* pp. 165-171.

[14] A. Pandey, N. Dasgupta and A. K. Mukerjee, "Design Issues in Implementing MPPT for Improved Tracking and Dynamic Performance", *IECON 2006 – IEEE 32nd Annual Conference on Industrial Electronics*, Paris, 2006, pp. 4387-4391.

[15] F. Liu, S. Duan, F. Liu, B. Liu and Y. Kang, "A Variable Step Size INC MPPT Method for PV Systems", *IEEE Transactions on Industrial Electronics,* vol. 55, nº 7, pp. 2622-2628, 2008.

[16] Y. Ou, C. Wang and F. Hong, "A Variable Step Maximum Power Point Tracking Method Using Taylor Mean Value Theorem", *2010 Asia-Pacific Power and Energy Engineering Conference*, Chengdu, 2010, pp. 1-4.

[17] Q. Mei, M. Shan, L. Liu and J. M. Guerrero, "A Novel Improved Variable Step-Size Incremental-Resistance MPPT Method for PV Systems", *IEEE Transactions on Industrial Electronics,* vol. 58, nº 6, pp. 2427-2434, June 2011.

[18] N. E. Zakzouk, A. K. Abdelsalam, A. A. Helal and B. W. Williams, "Modified variable-step incremental conductance maximum power point tracking technique for photovoltaic systems", *Industrial Electronics Society, IECON 2013 - 39th Annual Conference of the IEEE*, 2013, Vienna, 2013, pp. 1741-1748.

[19] S. Satapathy, K. M. Dash and B. C. Babu, "Variable step size MPPT algorithm for photo voltaic array using zeta converter - A comparative analysis", *Engineering and Systems (SCES), 2013 Students Conference on*, 2013, pp. 1-6.

[20] S. K. Kollimalla and M. K. Mishra, "Variable Perturbation Size Adaptive Perturb and Observe MPPT Algorithm for Sudden Changes in Irradiance", *IEEE Transactions on Sustainable Energy,* vol. 5, nº 3, pp. 718-728, July 2014.

[21] A. Morales-Acevedo, J. L. Díaz-Bernabé and R. Garrido-Moctezuma, "Improved MPPT adaptive incremental conductance algorithm", *IECON 2014 - IEEE 40th Annual Conference of the Industrial Electronics Society*, Dallas, TX, 2014, pp. 5540-5545.

[22] M. Killi and S. Samanta, "Modified Perturb and Observe MPPT Algorithm for Drift Avoidance in Photovoltaic Systems", *IEEE Transactions on Industrial Electronics,* vol. 62, nº 9, pp. 5549-5559, Sept 2015.

[23] Q. Li and P. Wolfs, "A Review of the Single Phase Photovoltaic Module Integrated Converter Topologies With Three Different DC Link Configurations", *IEEE Transactions on Power Electronics,* vol. 23, no. 3, pp. 1320-1333, May 2008.

[24] D. Sera, R. Teodorescu and P. Rodriguez, «PV panel model based on datasheet values», *2007 IEEE International Symposium on Industrial Electronics,* Vigo, Spain, 2007, pp. 2392-2396.

[25] D. Maksimovic, A. M. Stankovic, V. J. Thottuvelil and C.Verghese, "Modeling and simulation of power electronic converters", *IEEE Proceeding,* vol. 89, nº 6, pp. 898-911, June 2001.

[26] R. W. Erickson and D. Maksimovic, "State Space Averaging" in *Fundamentals of Power Electronics*, Second ed., Springer Science and Media Publishers, 2001, ch. 7, pp. 213-225.

[27] P. N. Enjeti and W. Shireen, "A new technique to reject DC-link voltage ripple for inverters operating on programmed PWM waveforms", *IEEE Transactions on Power Electronics,* vol. 7, no. 1, pp. 171-180, Jan 1992.

[28] T. Brekken, N. Bhiwapurkar, M. Rathi, N. Mohan, C. Henze and L. R. Moumneh, "Utility-connected power converter for maximizing power transfer from a photovoltaic source while drawing ripple-free current", in *2002 IEEE 33rd Annual Power Electronics Specialists Conference, pesc 02.*, vol.3, pp. 1518-1522.

[29] N. A. Ninad and L. A. C. Lopes, "Operation of Single-phase Grid-Connected Inverters with Large DC Bus Voltage Ripple", *2007 IEEE Electrical Power Conference, EPC 2007,* Montreal, Que., 2007, pp. 172-176.

[30] F. Gao, D. Li, P. C. Loh, Y. Tang and P. Wang, "Indirect dc-link voltage control of two-stage single-phase PV inverter," *2009 IEEE Energy Conversion Congress and Exposition*, San Jose, CA, 2009, pp. 1166-1172.

[31] Mohan, Ned, and Tore M. Undeland. "DC-DC Switch mode converters" in *Power electronics: converters, applications, and design*. Second Ed., John Wiley & Sons, 1989, ch. 7, pp. 190-192.

[32] S. Buso and P. Mattavelli, "The Test Case: a single-phase voltage source inverter" in *Digital Control in Power Electronics*, Morgan & Claypool, 2006, ch. 2, pp. 15-16.

[33] M. Ciobotaru, R. Teodorescu and F. Blaabjerg, "Control of single-stage single-phase PV inverter", in *2005 European Conference on Power Electronics and Applications*, Dresden, 2005, pp. P.1-P.10.

[34] H. Hu, S. Harb, N. Kutkut, I. Batarseh and Z. J. Shen, "A Review of Power Decoupling Techniques for Microinverters With Three Different Decoupling Capacitor Locations in PV Systems", *IEEE Transactions on Power Electronics,* vol. 28, no. 6, pp. 2711-2726, June 2013.

[35] J. L. Díaz-Bernabé and A. Morales-Acevedo, "Photovoltaic module simulator implemented in SPICE and Simulink", *2015 12th International Conference on Electrical Engineering, Computing Science and Automatic Control (CCE)*, Mexico City, 2015, pp. 554-558.

.

978-1-5090-3511-3/16/$31.00 ©2016 IEEE